



HAL
open science

Magnetoelastic excitation spectrum in the rare-earth pyrochlore $\text{Tb}_2\text{Ti}_2\text{O}_7$

M. Ruminy, S. Guitteny, J. Robert, L.-P. Regnault, M. Boehm, P. Steffens, H. Mutka, J. Ollivier, U. Stuhr, J. White, et al.

► **To cite this version:**

M. Ruminy, S. Guitteny, J. Robert, L.-P. Regnault, M. Boehm, et al.. Magnetoelastic excitation spectrum in the rare-earth pyrochlore $\text{Tb}_2\text{Ti}_2\text{O}_7$. *Physical Review B*, 2019, 99 (22), pp.224431. 10.1103/PhysRevB.99.224431 . hal-02393407

HAL Id: hal-02393407

<https://hal.science/hal-02393407>

Submitted on 24 Aug 2023

HAL is a multi-disciplinary open access archive for the deposit and dissemination of scientific research documents, whether they are published or not. The documents may come from teaching and research institutions in France or abroad, or from public or private research centers.

L'archive ouverte pluridisciplinaire **HAL**, est destinée au dépôt et à la diffusion de documents scientifiques de niveau recherche, publiés ou non, émanant des établissements d'enseignement et de recherche français ou étrangers, des laboratoires publics ou privés.

Magnetoelastic excitation spectrum in the rare-earth pyrochlore $\text{Tb}_2\text{Ti}_2\text{O}_7$

M. Ruminy,¹ S. Guitteny,² J. Robert,^{2,*} L.-P. Regnault,^{3,4} M. Boehm,⁴ P. Steffens,⁴ H. Mutka,⁴ J. Ollivier,⁴ U. Stuhr,¹ J. S. White,¹ B. Roessli,¹ L. Bovo,⁵ C. Decorse,⁶ M. K. Haas,^{7,†} R. J. Cava,⁷ I. Mirebeau,² M. Kenzelmann,⁸ S. Petit,^{2,‡} and T. Fennell^{1,§}

¹Laboratory for Neutron Scattering and Imaging, Paul Scherrer Institut, 5232 Villigen PSI, Switzerland

²Laboratoire Léon Brillouin, CEA Saclay, Bâtiment 563, 91191, Gif-sur-Yvette Cedex, France

³Service de Physique Statistique, Magnétisme et Supraconductivité, UMR-E9001, CEA-INAC/UJF, 17 rue des Martyrs, 38054 Grenoble Cedex 9, France

⁴Institut Laue Langevin, CS 20156, Cedex 9, 38042 Grenoble, France

⁵London Centre for Nanotechnology and Department of Physics and Astronomy, University College London, 17-19 Gordon Street, London, WC1H 0AH, United Kingdom

⁶ICMMO, Université Paris-Sud, Université Paris-Saclay, F-91405 Orsay, France

⁷Department of Chemistry, Princeton University, Princeton, New Jersey 08540, USA

⁸Laboratory for Developments and Methods, Paul Scherrer Institut, 5232 Villigen PSI, Switzerland



(Received 25 February 2019; revised manuscript received 21 May 2019; published 28 June 2019)

$\text{Tb}_2\text{Ti}_2\text{O}_7$ presents an ongoing conundrum in the study of rare-earth pyrochlores. Despite the expectation that it should be the prototypical unfrustrated noncollinear Ising antiferromagnet on the pyrochlore lattice, it presents a puzzling correlated state that persists to the lowest temperatures. Effects which can reintroduce frustration or fluctuations are therefore sought, and quadrupolar operators have been implicated. One consequence of strong quadrupolar effects is the possible coupling of magnetic and lattice degrees of freedom, and it has previously been shown that a hybrid magnetoelastic mode with both magnetic and phononic character is formed in $\text{Tb}_2\text{Ti}_2\text{O}_7$ by the interaction of a crystal field excitation with a transverse-acoustic phonon. Here, using polarized and unpolarized inelastic neutron scattering, we present a detailed characterization of the magnetic and phononic branches of this magnetoelastic mode, particularly with respect to their composition, the anisotropy of any magnetic fluctuations, and also the temperature dependence of the different types of fluctuation that are involved. We also examine the dispersion relations of the exciton branches that develop from the crystal field excitation in the same temperature regime that the coupled mode appears, and find three quasidispersionless branches where four are expected, each with a distinctive structure factor indicating that they are nonetheless cooperative excitations. We interpret the overall structure of the spectrum as containing four branches, one hybridized with the phonons and gaining a strong dispersion, and three remaining dispersionless.

DOI: [10.1103/PhysRevB.99.224431](https://doi.org/10.1103/PhysRevB.99.224431)

I. INTRODUCTION

The members of the rare-earth pyrochlore series $R_2\text{Ti}_2\text{O}_7$ exhibit strikingly different magnetic behaviors [1,2]. Their diversity originates in the interplay of crystal field effects, spin interactions, and geometric frustration. For $\text{Tb}_2\text{Ti}_2\text{O}_7$, given these ingredients, two basic predictions are a transition to long-range magnetic order, or a cooperative Jahn-Teller transition to a nonmagnetic state. However, neither occurs; instead, depending on the sample, either a correlated, fluctuating state described as a spin liquid persists down to the lowest temperatures studied or a hidden-order transition to a possible multipole-ordered state occurs [3–5]. The general problems in $\text{Tb}_2\text{Ti}_2\text{O}_7$ are to understand the nature of these states, to identify how they are stabilized, and to establish if they have

any particularly interesting properties such as the emergent phenomena which have become topical in the closely related (quantum) spin ices [6,7]. Here, we investigate the possible role of coupling between spin and lattice fluctuations by making a detailed experimental characterization of the recently discovered magnetoelastic mode (MEM) [8,9].

The crystal structure of $\text{Tb}_2\text{Ti}_2\text{O}_7$ contains two pyrochlore lattices, one formed by magnetic Tb^{3+} ions, and a second one formed by nonmagnetic Ti^{4+} ions. The 7F_6 free-ion term of Tb^{3+} is split by a crystal electric field with D_{3d} symmetry and various investigations of the crystal field scheme agree that the ground state is a non-Kramers doublet with Ising character [10–16], so that the magnetic moments are constrained to the local noncollinear $\langle 111 \rangle$ axes (the body axes of the tetrahedra) at low temperature. The Curie-Weiss temperature suggests that the interactions are antiferromagnetic, as $\theta_{\text{CW}} = -13$ K [10]. On the pyrochlore lattice, classical $\langle 111 \rangle$ spins interacting by near-neighbor antiferromagnetic Heisenberg exchange have a fully ordered, nondegenerate ground state of the “four-in–four-out” type [17,18], hence, the expectation of long-range magnetic order in $\text{Tb}_2\text{Ti}_2\text{O}_7$. The other simple

*Now at CNRS, Institut Néel, 38042 Grenoble, France.

†Now at Air Products and Chemicals Inc., Allentown, PA 18195.

‡sylvain.petit@cea.fr

§tom.fennell@psi.ch

expectation, a structural distortion due to a cooperative Jahn-Teller effect (CJTE), is possible since the unprotected degeneracy of the non-Kramers doublets makes them, in principle, Jahn-Teller active. Indeed, terbium compounds provide some of the canonical examples of CJTEs [19].

As mentioned, neither of these possibilities occurs, and the exact low-temperature behavior is somewhat obscured by sample-dependent properties such as the presence or absence of a heat capacity anomaly [3,20–22], or different (partial) spin freezing temperatures [21–25]. Such sample dependence in rare-earth pyrochlores is typically attributed to very small levels of off stoichiometry [26], and detailed experimental work on samples in which the exact stoichiometry is varied according to $\text{Tb}_{2+x}\text{Ti}_{2-x}\text{O}_{7+y}$ [3–5,27–33] suggests that for a small range of $-0.05 \lesssim x \lesssim 0.04$, a phase transition that is not of magnetic dipole or structural origin (i.e., a hidden order) appears at $T \approx 0.5$ K and everywhere outside this critical compositional range, the spin liquid develops.

Construction of a theory of $\text{Tb}_2\text{Ti}_2\text{O}_7$ is difficult since the character of the basic degree of freedom is changing as its interactions become important; a crystal field level at 1.5 meV means that the local anisotropy [34,35] and spin correlations [5,11,36–41] develop simultaneously below $T \approx 20$ K. A theory based on Heisenberg exchange and the admixing of this level by virtual crystal field excitations (VCFEs) predicted that $\text{Tb}_2\text{Ti}_2\text{O}_7$ is a type of quantum spin ice [42–44], with a magnetization plateau when the field is applied along the [111] direction [44]. However, there is disagreement about the evidence for this plateau [45–49], which may exist at very low temperature ($T \sim 0.02$ K) [48], but is lost even at typical dilution fridge temperatures ($T \sim 0.07$ K) [49]. In any case, it is not as prominent as predicted. On the other hand, a theory in which pseudo- $(S = \frac{1}{2})$ derived from the single-ion ground-state doublet (i.e., neglecting any role of higher states) [27,29] interact by generalized anisotropic near-neighbor superexchange interactions [50–53] that couple dipole and quadrupole moments suggests that the hidden order is a quadrupolar ordering [29]. This theory is reasonably successful in accounting for thermodynamic properties and the development of a weakly dispersive excitation with a gap of $\Delta \sim 0.07$ meV in the region of the transition [27,29]. By comparison with the phases of the same theory [29], it is suggested that the spin liquid is a U(1) spin liquid [7,54,55], and that the presence of a pinch point in the diffuse scattering [37] implies it is connected [5] to the predicted quantum spin ice [43]. However, other experimental phenomena, such as the small ordered magnetic moment in the hidden-order phase and the form of the diffuse scattering of the spin-liquid phase [5], cannot be explained, and the application of theories of quantum effects in pyrochlores with isolated doublet ground states [51–53,56] to $\text{Tb}_2\text{Ti}_2\text{O}_7$ may not be entirely successful because of the low-lying level [42,43].

An alternative theory based on a splitting of the ground-state doublet into two singlets by a hypothetical static [57] or dynamical [58] Jahn-Teller distortion has been compared with a comprehensive neutron diffraction experiment, and reproduces well the observed magnetization curve without plateau (at $T \approx 0.07$ K) [49], it also quite successfully reproduces the diffuse scattering [38]. However, it has been criticized because there is no clear structural [59–63] or spectroscopic [64,65]

evidence for any distortion, and because it cannot reproduce either the large elastic magnetic spectral weight [65] or the hyperfine contribution to the specific heat [22], both of which require a permanent magnetic moment at the terbium site.

Each description of $\text{Tb}_2\text{Ti}_2\text{O}_7$ has its own merits, but none is completely successful, which could imply that there are other important effects to be incorporated. Notably, all the above observations and theories concern only the “magnetic sector,” so that a potentially important actor in the physics of $\text{Tb}_2\text{Ti}_2\text{O}_7$, the lattice and its coupling to the rare-earth ions, is ignored. In fact, magnetoelastic interactions in $\text{Tb}_2\text{Ti}_2\text{O}_7$ have been manifested for as long as the material has been studied. Studies of the Young’s modulus [66,67] and elastic constants [68] show that they soften anomalously at low temperature, suggesting a CJTE at 0.1 K, below the temperature range of the study. Later, a systematic search for a distortion using x-ray diffraction down to 0.3 K was made, and although various Bragg peaks were observed to broaden as if approaching a cubic to tetragonal distortion, no distortion actually occurred [60]. Other x-ray diffraction [61,62], neutron Larmor diffraction [63], and thermal expansion [69] experiments have corroborated the absence of a low-temperature distortion down to at least 0.5 K, but show unusual thermal expansion behavior below 20 K.

These effects are all measured in the “structural sector.” It is their temperature dependence that betrays the connection between spins and lattice: all the anomalous lattice effects build up below 20 K, exactly in the temperature range where the spin correlations also develop, and as the first excited crystal field level is depopulated. More recently, it has been shown by inelastic neutron scattering that a hybrid excitation (described more fully below) formed by the mixing of transverse-acoustic phonons and crystal field excitations appears exactly in the same temperature range [8]. Two other groups of measurements outside the zero field, ambient pressure, low-temperature state, one of pressure- and strain-induced magnetic order [70,71], and one of structural modifications induced by (very large) magnetic fields [72], also point to the strong coupling of the spin and lattice. The mixing of spin and lattice fluctuations and the underlying involvement of quadrupole operators may be a part of the solution to the puzzle of $\text{Tb}_2\text{Ti}_2\text{O}_7$ that has not yet been fully investigated.

In the following, we summarize separately the main features of the inelastic neutron scattering spectrum of $\text{Tb}_2\text{Ti}_2\text{O}_7$ for reference (Sec. II), before presenting the experimental methods (Sec. III), and results of neutron scattering experiments (Sec. IV), which are subsequently discussed (Sec. V).

II. NEUTRON SPECTRUM OF $\text{Tb}_2\text{Ti}_2\text{O}_7$ AND THE MAGNETOELASTIC MODE

Since we will be discussing the neutron inelastic scattering spectrum of $\text{Tb}_2\text{Ti}_2\text{O}_7$ at some length, we summarize here its features. The energy transfer may be broadly described as elastic, quasielastic, or inelastic. Here, we are only concerned with inelastic scattering. The momentum transfer \vec{Q} may be moderate or large. Generally, in $\text{Tb}_2\text{Ti}_2\text{O}_7$ the inelastic regime contains magnetic excitations, particularly crystal field excitations, at moderate momentum transfer where the magnetic form factor is large, and phonons at large momentum transfer

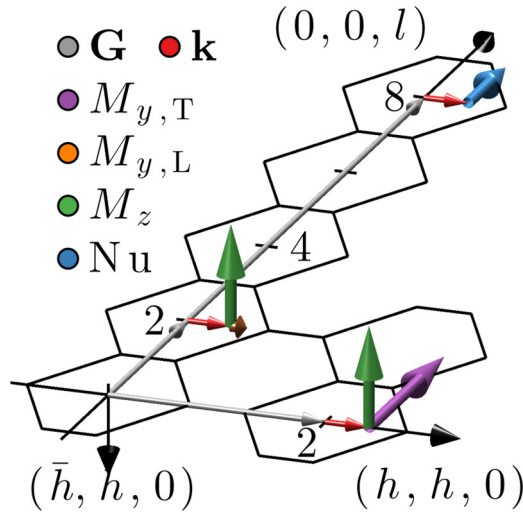


FIG. 1. Comparison of measurement of fluctuations contributing to the MEM. With $\vec{k} \parallel (h, h, 0)$ at $(2, 2, 0)$ the magnetic branch has both $M_{y,T}$ and M_z transverse to \vec{k} and also measurable since they are perpendicular to $\vec{Q} = \vec{G} + \vec{k}$. At $(0, 0, 2)$ with $\vec{k} \parallel (h, h, 2)$ the magnetic branch has $M_{y,L}$ longitudinal and M_z transverse to \vec{k} but measurable since they are both dominantly perpendicular to $\vec{Q} = \vec{G} + \vec{k}$. The phonon branch has the character of a TAP and appears at $(0, 0, 8)$, where lattice or nuclear fluctuations (Nu) are transverse to \vec{k} but dominantly parallel to $\vec{Q} = \vec{G} + \vec{k}$.

where the $|\vec{Q}|^2$ dependence of the phonon cross section makes it dominant. There are two crystal field levels within the scope of this study: the first excited state at $\hbar\omega \simeq 1.5$ meV (CEF1) and the second at $\hbar\omega \simeq 10$ meV (CEF2), a doublet and a singlet, respectively. Below 20 K, CEF1 becomes dispersive [11], which implies that magnetic interactions couple the crystal field excitations, allowing them to propagate. In this situation, crystal field excitations are more correctly known as excitons, and we refer to the modes derived from the crystal field level as exciton branches. It was suggested that CEF1 contains two branches [8].

At moderate \vec{Q} , intersecting with CEF1 is a weak, sharp mode with dispersion strongly reminiscent of an acoustic phonon [8]. Phonons are not expected at these momentum transfers, and indeed polarized neutron scattering showed that this mode is magnetic. However, a time-of-flight data set providing simultaneous access to moderate and large \vec{Q} showed that the magnetic mode has the same dispersion relation as a mode that was argued to be a transverse-acoustic phonon (TAP). Since the two have the same dispersion relation, it was suggested that they are the same excitation: a magnetoelastic mode (MEM) with different selection rules for the magnetic and phononic parts. Although we usually refer to the magnetic part as the MEM and the phonon part as a TAP, in reality when the crystal field and phonon excitations are coupled, they are the magnetic and phononic branches of the same hybrid excitation.

The relationship between different magnetic and phonon fluctuations is sketched in Fig. 1. The MEM was observed close to $(2, 2, 0)$ where it propagates along $(h, h, 0)$. Neutron scattering is sensitive to spin components perpendicular to the scattering vector \vec{Q} , which may be resolved into those

lying in the scattering plane M_y , and perpendicular to it M_z , by polarization analysis. When the propagation vector \vec{k} of the mode is parallel to \vec{Q} (and hence the spin components involved are perpendicular to \vec{k}), we call both M_y and M_z transverse spin fluctuations. The phononic part was observed close to $(0, 0, 8)$, where it propagates along $(h, h, 8)$. With its propagation direction \vec{k} perpendicular to \vec{Q} , appearing at large momentum transfer, this part has the hallmarks of a TAP. In a polarization analysis experiment, it will appear as nuclear scattering. The transverse/longitudinal descriptors we use are analogous to those employed in studies of phonons, in which they describe the relationship between lattice fluctuations and \vec{k} . Usually, in magnetism, spin-wave excitations are called transverse because they are transverse fluctuations of the ordered moment, while longitudinal excitations are fluctuations of the amplitude of the ordered moment. Here, with no ordered structure, this description has no particular meaning. Furthermore, we can investigate a longitudinal magnetoelastic fluctuation involving spin components which fluctuate parallel to \vec{k} , for example, at $(0, 0, 2)$, with $\vec{k} = (h, h, 2)$, the M_y fluctuations are perpendicular to \vec{Q} and parallel to \vec{k} .

The classification of the magnetic fluctuation directions derives from the usual description of the neutron polarization in a frame of reference relative to the scattering vector \vec{Q} . The neutron polarization is parallel to x when it is parallel to \vec{Q} (which is in the horizontal plane of the experiment), parallel to z when it is vertical (and hence perpendicular to \vec{Q}), and parallel to y when it is in the mutually perpendicular direction that lies in the scattering plane. We measure neutron scattering events in different polarization channels depending if the neutron spin is not flipped (non-spin flip, NSF, P_x , P_y , or P_z) or is flipped (spin flip, SF, P'_x , P'_y , P'_z). Magnetic moment components perpendicular to the scattering vector and parallel (perpendicular) to the polarization scatter neutrons in the relevant nonspin-flip (spin-flip) channel. Fluctuations of the magnetic moments perpendicular to the scattering vector and in the scattering plane appear in P'_x , P_y , and P'_z ; fluctuations of the magnetic moments perpendicular to the scattering vector and perpendicular to the scattering plane appear in P'_x , P'_y , and P_z ; phonons appear in P_x , P_y , and P_z . The combination of P_x and P'_x is ideal for separating phononic and magnetic contributions, while comparison of P_z and P_y (in this case) can be used to investigate anisotropy of magnetic fluctuations between the in- and out-of-plane directions (other combinations can be used for the same purpose). The contributions to the different polarization channels are summarized in Table I.

For the purpose of this study, single crystals of $\text{Tb}_2\text{Ti}_2\text{O}_7$ studied by inelastic neutron scattering, no sample dependence has so far been evidenced. The dispersion of the first crystal field level and its exciton branches can be seen in various reports, and appears to be identical [8,11,36,73]. The magnetoelastic mode investigated here appears in several samples with and without the specific heat peak, and has been shown to have the same form and temperature dependence in a collection of crystals with slightly different lattice parameters and specific heat behaviors [8,9,74]. Reports of the low-energy scattering are much more variable, including descriptions of gapless, gapped and propagating excitations [3,9,11,12,22,29,33,36,39,40,64,65,75]. Very fine

TABLE I. Summary of the direct-space magnetic moments whose fluctuations give rise to the scattering in the various polarization channels mentioned in the text. The T and L designations for $(h, h, 0)$ distinguish transverse [T, measured with $k \parallel (h, h, 0)$ at $(2, 2, 0)$] and longitudinal [L, measured with $k \parallel (h, h, 0)$ at $(0, 0, 2)$] fluctuations, as also described in the text. The P'_y and P'_z channels were not used, but contain the same magnetic information as P_y and P_z but exchanged, P_y and P_z also contain nuclear (N) scattering, and each pair of nonspin-flip/spin-flip channels contains spin incoherent scattering in the ratio $1/3 : 2/3$.

\vec{k}	P_x	P'_x	P_y	P_z
$(h, h, 0)$ (T)	N	$M_y + M_z$	$M_y = [001]$	$M_z = [1\bar{1}0]$
$(h, h, 0)$ (L)	N	$M_y + M_z$	$M_y = [110]$	$M_z = [1\bar{1}0]$
$(0, 0, l)$	N	$M_y + M_z$	$M_y = [110]$	$M_z = [1\bar{1}0]$
(h, h, h)	N	$M_y + M_z$	$M_y = [\bar{1}\bar{1}2]$	$M_z = [1\bar{1}0]$

energy resolution and polarization analysis [9] appear to be essential for a full understanding, and it is much more difficult to make meaningful comparisons amongst reports. However, particularly with reference to recent reports of samples with controlled stoichiometry, it does appear that in the very low-energy sector, single-crystal neutron scattering is sensitive to a sample-dependent property. In this paper, we do not attempt to resolve this issue since we do not present any measurements which are relevant to this energy scale.

III. EXPERIMENTAL METHODS

A. Samples

We have used two single-crystal samples in this study, one grown in Princeton (A) and one in Paris (B); both have been studied and described before [8,9,37,38,74]. MEMs were characterized in some detail in sample A [8,74] (which is also called MH1 in Ref. [74]), and are also clearly visible in sample B [9] (which is also called CEA in Ref. [74]). Further detailed comparisons of the two samples are made in the Supplemental Material [76]. Sample A was a single crystal of mass ~ 7 g. It was held in a copper mount that clamped the sample at one end during the experiments using time-of-flight (TOF) and (polarized and unpolarized) triple-axis (TAS) spectrometers originally reported in Ref. [8], and for the polarized TAS experiments described here in Secs. III B, IV A, IV B, and IV E. It was later held in a full clamp designed to immobilize it in applied field, which proved advantageous since the sample cracked into two approximately equal sized pieces, though these remained clamped in close coalignment and the sample was used in that configuration for further unpolarized thermal TAS experiments described in Secs. III C and IV C. Sample B was also used in TOF and polarized TAS experiments originally presented in Ref. [9], where it comprised four coaligned single crystals of $\text{Tb}_2\text{Ti}_2\text{O}_7$ with total mass ~ 11 g, each held by a copper clamp at one end. Subsequently, two of these crystals were used for the polarized TAS experiments described in Secs. III D, IV D, and IV E.

B. Thermal triple-axis spectroscopy with Cryopad (IN22)

Anisotropic magnetic and phononic components of the magnetoelastic fluctuations were measured on the thermal

TAS IN22 at the ILL in combination with the spherical neutron polarimetry device CryoPAD [77,78]. The crystal (sample A) was held in a copper clamp with the $[1\bar{1}0]$ axis perpendicular to the horizontal plane and loaded into a dilution refrigerator insert, which was cooled in a dedicated ‘‘Orange’’ cryostat that matches the internal sizes of the Cryopad. Using Heusler (1, 1, 1) monochromator [vertical focusing 140×120 mm (width \times height), 30' mosaic] and analyzer (horizontal focusing, 150×100 mm, 30' mosaic), open collimation, and a pyrolytic graphite (PG) filter, the spectrometer was operated at the fixed final energies $E_f = 14.68$ meV ($k_f = 2.662 \text{ \AA}^{-1}$) or 34.83 meV ($k_f = 4.1 \text{ \AA}^{-1}$). The flipping ratio was ≈ 17 . Different combinations of the non-spin flip channels P_x, P_y, P_z and spin flip P'_x, P'_y, P'_z were recorded during constant energy scans at $\hbar\omega = 5$ meV or $\hbar\omega = 7$ meV across the MEM and TAP. Additionally, full polarization information was collected in single-point measurements at peak and background positions of the MEM. All measurements were performed at the base temperature of the dilution fridge, which was $T = 0.07$ K.

C. Unpolarized triple-axis spectroscopy (EIGER and TASP)

Subsequent measurements of the frequency and temperature dependence of the MEM and TAP were performed using unpolarized neutrons on the thermal neutron TAS EIGER [79] at SINQ, PSI. Sample A was clamped in a copper mount, but in the same orientation as used on IN22, and mounted in a dilution fridge (which was inserted into a 9-T cryomagnet.) The spectrometer was operated using a PG002 monochromator (double focusing, 300×180 mm, 30' mosaic) and analyzer (horizontal focusing, 170×150 mm, 30' mosaic) and open collimation, at fixed final energy $E_f = 14.68$ meV (with PG filter in the scattered beam) for measurements of the magnetic components and $E_f = 18.65$ meV ($k_f = 3 \text{ \AA}^{-1}$, PG filter removed) for measurements of the TAP. The frequency dependence was established from constant energy scans across the MEM at various energies $\hbar\omega > 3$ meV at $T = 0.07$ K, the base temperature of the dilution insert. The temperature dependence of the TAP was measured in a separate experiment, using the same sample in the same orientation, but mounted in a standard (‘‘Orange’’) helium cryostat. The magnetic fluctuations were accessed with constant energy scans along $\vec{k} = (h, h, 0)$ in the BZ of $\vec{Q} = (2, 2, 0)$, while the transverse lattice vibrations were accessed with constant energy scans along $\vec{k} = (h, h, 0)$ in the BZ of $\vec{Q} = (0, 0, 8)$ at $\hbar\omega = 7$ meV in a temperature range of $1.5 \leq T \leq 200$ K.

The frequency dependence of the magnetic part of the MEM was extended to lower energies using unpolarized neutrons on the cold neutron TAS TASP at SINQ, PSI, where sample A was mounted in the same cryogenic environment as on EIGER. Using PG(002) monochromator (vertical focusing, 150×125 mm, 30' mosaic) and analyzer (horizontal focusing, 150×150 mm, 30' mosaic), open collimation, and a cooled beryllium filter after the sample position, the spectrometer was operated at fixed final energy $E_f = 5$ meV. The magnetic fluctuations of the MEM were accessed with constant energy scans along $\vec{k} = (h, h, 0)$ in the BZ of $\vec{Q} = (2, 2, 0)$ at various energy transfers above the intense CEF1 excitation.

D. Cold TAS with Cryopad (IN14)

Using the cold neutron TAS IN14 at the ILL in combination with CryoPAD, the magnetic fluctuations of the CEF1 excitation were analyzed. This experiment was performed on sample B, aligned with the horizontal plane containing (h, h, l) scattering vectors. The sample was mounted in a dilution fridge, which was inserted in a helium cryostat. The spectrometer was configured with the PG002 monochromator (vertical focusing, 150×120 mm, $30'$ mosaic), supermirror bender polarizer ($\approx 40'$) and otherwise open collimation, Heusler (1, 1, 1) analyzer (horizontal focusing, 75×75 mm, $35'$ mosaic) and a cooled beryllium filter after the sample position, and operated at fixed final energy with $E_f = 4.66$ meV ($k_f = 1.5 \text{ \AA}^{-1}$). At selected points along the $(h, h, 0)$ direction, constant wave-vector scans were performed across the broad and dispersive CEF1 envelope, recording data in all three NSF channels to identify magnetic fluctuations in the y and z directions.

IV. RESULTS

We have addressed various experimental questions concerning the properties of the CEF1 and MEM excitations which remain unresolved after previous works, with a view to establishing the salient features of the coupling mechanism. In the following, we first present qualitatively simple results which reinforce or clarify findings from the previous works: explicit demonstration of MEMs in all high-symmetry directions, direct verification of magnetic and phononic parts, energy and temperature dependence of magnetic and phononic parts. We then address more complicated questions which have not been broached before: full structure of the CEF1 excitons, and the anisotropy of MEM magnetic fluctuations.

A. Existence of the magnetoelastic mode in different zones

The characterization of the MEM reported in Ref. [8] is dominated by investigations around the $(2, 2, 0)$ zone center, though the mode was also reported at $(1, 1, 1)$, propagating along (h, h, h) . In Ref. [9] the MEM was also visible in sample B at $(1, 1, 1)$, but was described as an acoustic phonon. The TOF data for sample A also suggested that the mode can be found at $(0, 0, 2)$, where the top of the dispersion appears to be visible, but it is extremely weak. Using a thermal TAS with polarization analysis and sample A, we confirmed the existence of a magnetic mode at $(1, 1, 1)$ and were also easily able to locate a magnetic mode propagating along $(0, 0, l)$ at $(0, 0, 2)$. As shown in Fig. 2, it can be seen that MEMs propagate in all the main symmetry directions.

B. Direct verification of magnetic and phononic components

In Ref. [8], it was stated that the MEM is formed by coupling CEF1 and a TAP. This conclusion was drawn from the evident interaction of the MEM with the crystal field excitation, and because the MEM has the same dispersion as the phonon in question. The magnetic character of the MEM was explicitly established using polarization analysis on the branch at $(2, 2, 0)$, but the other branch was deduced to be phononlike because it appears at large momentum transfer

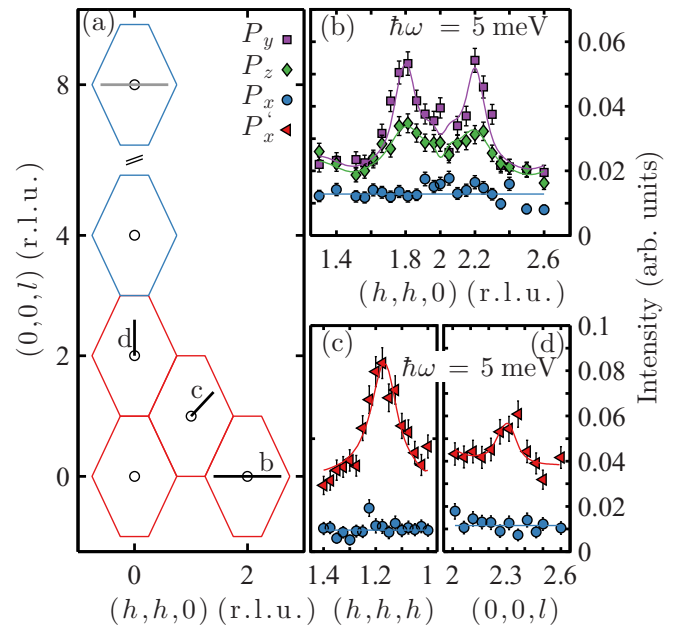


FIG. 2. Schematic overview of \vec{Q} and \vec{k} used to observe MEMs (a) and scans of MEMs at $(2, 2, 0)$ (b), $(1, 1, 1)$ (c), and $(0, 0, 2)$ (d). Scattering in the P_x channel is purely nuclear (i.e., phononic) in origin, P_y and P_z will contain the same nuclear contribution as P_x , plus magnetic contribution, while P'_x contains the total magnetic contributions found in P_y and P_z . The absence of any peak in P_x accompanied by peaks in either P_y , P_z , or P'_x shows that all these signals are magnetic.

$[\vec{Q} = (h, h, 8)]$ with propagation direction $\vec{k} \perp \vec{Q}$. Using a thermal TAS with polarization analysis, we could access both branches and confirm directly that the one we observe at $(2, 2, 0)$, with $\vec{k} \parallel \vec{Q}$ [i.e., along $(h, h, 0)$] is purely magnetic scattering, while the branch we observe at $(0, 0, 8)$ with $\vec{k} \perp \vec{Q}$ [i.e. along $(h, h, 8)$] is nuclear scattering, i.e., phononic. Furthermore, by measuring the longitudinal-acoustic phonon (LAP) along $(h, h, 0)$ at $(4, 4, 0)$ we confirmed that it is only the TAP which plays a role, as the LAP has a quite different dispersion. The comparison of MEM, TAP, and LAP can be seen in Fig. 3 [the full dispersion of the phonons can be found in Ref. [80], the magnetic component measured at $(0, 0, 2)$ along $(h, h, 2)$ is discussed below in Sec. IV E].

We also verified the same relation between MEM and TAP excitations for MEMs propagating along $(0, 0, l)$ at $(0, 0, 2)$ [with the TAP measured at $(4, 4, l)$] and (h, h, h) at $(1, 1, 1)$ [with the TAP measured along $(h, h, 2h)$ at $(5, 5, 5)$]. As shown in Fig. 4, the MEM has a corresponding TAP in all directions.

C. Frequency dependence of magnetoelastic mode and phonon intensities

In previous works, two contrasting behaviors of the frequency dependence of the magnetoelastic mode were reported. In Ref. [9] the intensity of the MEM just above CEF1 was extracted from TOF data and found to decay as $1/\hbar\omega$, while in Ref. [8] the intensity of the magnetic branches extracted from TOF data extending to higher energy was found to be approximately independent of frequency. Neither

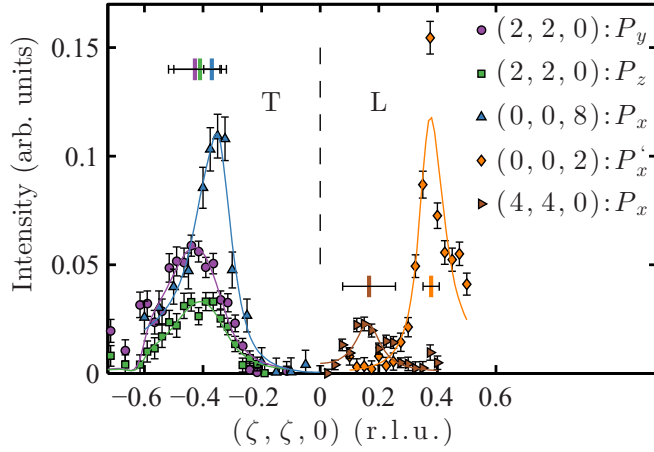


FIG. 3. Phononic and magnetic contributions to the magnetoelastic mode. In reduced wave vector, we find the transverse-acoustic phonon propagating along $(h, h, 8)$ at $(0, 0, 8)$ and appearing in the P_x channel appears (within the limits of our resolution fit given by the horizontal bars) at the same wave vector as the MEM propagating along $(h, h, 0)$ at $(2, 2, 0)$. The longitudinal-acoustic phonon propagating along $(h, h, 0)$ at $(4, 4, 0)$ and appearing in the P_x channel has a quite different dispersion. Magnetic components propagating along $(h, h, 2)$ at $(0, 0, 2)$ and appearing in the P'_x channel also have the same dispersion as the MEM and TAP. (All measurements at $\hbar\omega = 7$ meV.)

the existing TOF data (limited energy range or statistics), nor polarized TAS experiments (limited count rate) are completely suitable for determining this quantity. However, due to the natural separation of the nuclear and magnetic cross section of the MEM in the neutron excitation spectrum demonstrated above, we have obtained a clearer picture of

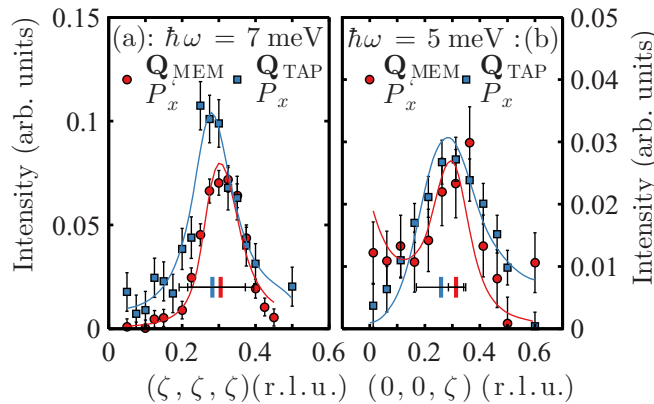


FIG. 4. Transverse-acoustic (TAP) and transverse-magnetic (MEM) contributions to the magnetoelastic mode propagating along different high-symmetry directions of the reciprocal lattice. (a) Magnetic (phononic) signal measured with $\vec{k} = (h, h, h)$ in the Brillouin zone $\vec{Q} = (1, 1, 1)$ and P'_x channel [$\vec{k} = (h, h, -h)$, $\vec{Q} = (3, 3, 7)$, P_x]. (b) Magnetic (phononic) signal measured with $\vec{k} = (0, 0, l)$ in the Brillouin zone $\vec{Q} = (0, 0, 2)$ and P'_x channel [$\vec{k} = (0, 0, l)$, $\vec{Q} = (4, 4, 0)$, P_x]. In both cases, a transverse-acoustic phonon signal appears at the same reduced wave vector as the magnetic fluctuation.

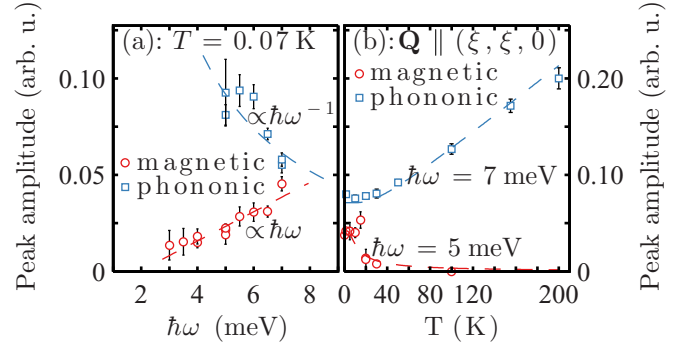


FIG. 5. Intensity of the magnetic and phononic contributions to the magnetoelastic mode as a function of energy transfer $\hbar\omega$ (a) and temperature T (b). Dashed lines in (a) are guides to the eye following the indicated $\hbar\omega$ dependence, dashed lines in (b) are the expected temperature dependence of a phonon mode obeying Bose statistics (measured at $\hbar\omega = 7$ meV), and the intensity of the MEM controlled by the Boltzmann population of CEF1 (measured at $\hbar\omega = 5$ meV) [8].

the magnetic and phononic components using unpolarized neutrons, as shown in Fig. 5.

The peak amplitudes were extracted from fitting a damped harmonic oscillator dispersion model (convoluted with the instrumental resolution function, which was evaluated using the Popovici algorithm [81] using RESCAL5 [82]) to the constant energy scans and are presented as function of energy transfer $\hbar\omega$ or temperature, respectively. These measurements confirm the $1/\hbar\omega$ dependence of the phononic branch (at $T = 0.07$ K). The peak amplitudes of the two points near $\hbar\omega = 6$ meV are difficult to estimate due to an overlap with a low-lying optical phonon [80]. In contrast, the peak amplitude of the magnetic component increases approximately linearly with $\hbar\omega$, which is clearly not compatible with a phonon excitation. Although the integrated intensities of the MEM previously extracted from TOF data collected at IN5 appeared to be independent of $\hbar\omega$, our new more precise measurements using a TAS adjust this picture: We show that the peak amplitude of the MEM increases approximately linearly with energy transfer, and is particularly large at $\hbar\omega = 7$ meV.

It was previously shown that the intensity of the magnetic component of the MEM follows the characteristic temperature law of the Boltzmann statistics of the lowest crystal field level CEF1 [8]. The temperature dependence of the peak amplitude of the TAP, in contrast, is well approximated by the temperature law of Bose-Einstein statistics, as shown in Fig. 5.

In short, the measurements of the frequency and temperature dependence confirm independently the phononic origin of the excitation in the BZ $(0, 0, 8)$. They also suggest that the phonon is rather classical, as its expected temperature and frequency dependence are not strongly perturbed by the development of the coupling with the spin system. The magnetic contribution to the hybrid modes displays an unconventional increase of intensity with increasing energy transfer.

D. Structure of exciton modes

It is known that the lowest-lying crystal field level of $\text{Tb}_2\text{Ti}_2\text{O}_7$ becomes dispersive at low temperature [11],

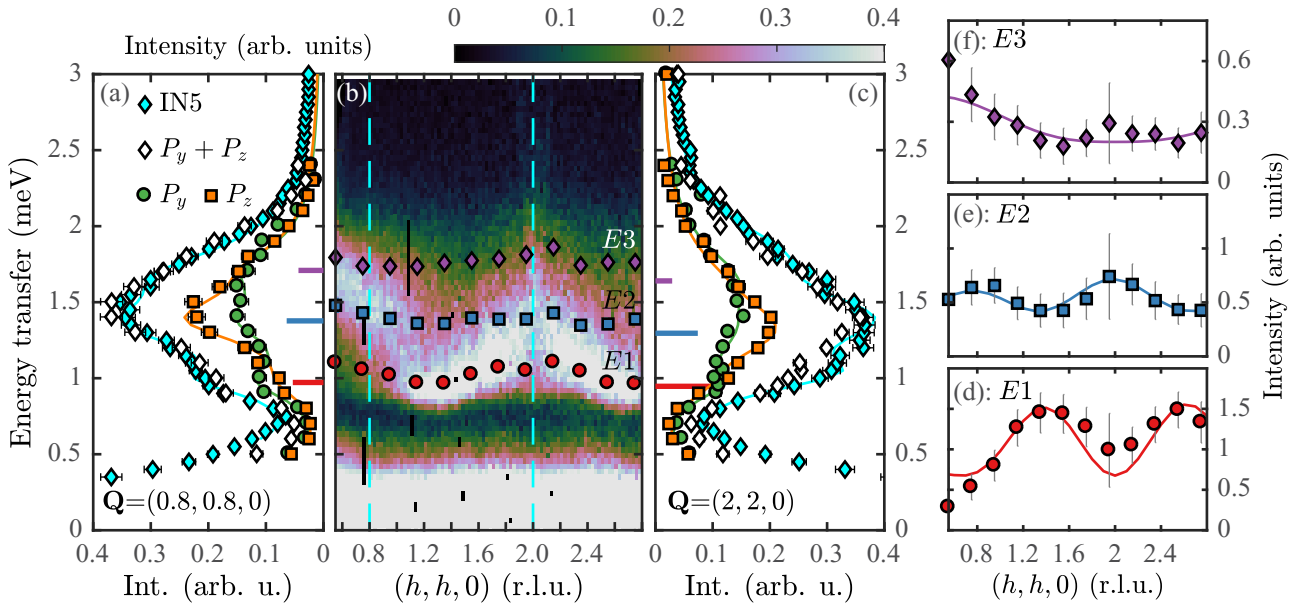


FIG. 6. The structure of the three exciton modes $E1$, $E2$, and $E3$ at $T = 0.07$ K, which develop from CEF1 at low temperature, along the $(h, h, 0)$ direction. (b) Shows a color map of the unpolarized time-of-flight neutron intensity. Cuts through the data along the cyan broken lines (TOF) are shown together with scans using polarized neutrons (P_y and P_z) in (a) and (c). Comparison of the P_y and P_z channels shows that the envelope of intensity in the unpolarized data contains three distinct peaks. The wave-vector dependence of the intensity of the modes $E1$ – $E3$ extracted by fitting three peaks to the unpolarized (TOF) data are shown in (d)–(f), where the lines are a guide to the eye. The extracted peak positions of the three exciton modes are the points superimposed on (b), and error bars on these positions are comparable to the symbol size.

indicating that magnetic interactions allow the single-ion crystal field excitations to propagate. In Ref. [8] part of the exciton dispersion was reported, and it was stated that the envelope of the exciton mode contained two branches. One was found to be rather sharp, and the other rather broad and asymmetric. To investigate the structure of the exciton branches at the point where they meet the strongly dispersing MEM, we studied the broad envelope of the CEF1 excitation using polarized neutrons. Our hypothesis was that there would be a clear separation in behavior between M_y and M_z fluctuations, allowing us to establish which parts of the exciton spectrum are hybridized with the TAP to form the MEM.

Our first finding when examining the exciton branches with polarized neutron scattering is unambiguous evidence that there are in fact three branches, as shown in Figs. 6(a) and 6(c). The three modes are not resolution limited and all appear in both magnetic P_y and P_z channels. Having used polarization analysis to identify that there are three modes, we can further examine their wave-vector dependence in the TOF data measured using sample A and originally presented in Ref. [8]. Fitting three modes to the TOF data shows that they have nearly wave-vector-independent dispersion relations, with a maximum bandwidth of ~ 0.1 meV for each branch, but strongly modulated intensities along the $(h, h, 0)$ direction, as shown in Figs. 6(b) and 6(d)–6(f). The fitting parameters were controlled by referring to the polarized TAS data where the modes can be individually distinguished. This wave-vector-dependent intensity modulation produces the broad and strongly dispersing “w”-shaped envelope in the unpolarized neutron scattering spectrum. We refer to the three modes as $E1$, $E2$, and $E3$ in the following.

We can perform a similar analysis using the TOF data in cuts along the $(0, 0, l)$ direction, where the intensity of CEF1 has previously been presented by Rule *et al.* [73] and shows a very striking wave-vector and energy dependence. As can be more clearly seen in Fig. 7(b), around $(0, 0, 2)$, the structure of CEF1 resembles a resonance, with modes appearing to disperse outward in both upward and downward directions. Cuts through the data [Figs. 7(a) and 7(c)] show the presence of three branches in the envelope, but fitting to a series of cuts along the $(0, 0, l)$ reveals that this structure comes from the wave-vector-dependent intensity modulation of the three quasispersionless branches.

Since we expected that the formation of the exciton branches would be accompanied by significant dispersion due to magnetic interactions, or conversely that nondispersive modes would be single-ion fluctuations with intensity modulated only by the Tb^{3+} magnetic form factor, this situation is somewhat surprising. In Fig. 8, we show the wave-vector dependence of the intensity of the three modes obtained from the time-of-flight data by assuming that they are dispersionless and integrating $S(\vec{Q}, \omega)$ between narrow limits of energy transfer. We will discuss the wave-vector dependence below.

Our second finding concerns the anisotropy of the fluctuations, and is presented in Fig. 9. The signal of the fluctuations is calculated from $M_y = P_y - P_x$ and $M_z = P_z - P_x$ with the polarization directions of the spin fluctuations therefore being along $[001]$ and $[1\bar{1}0]$, respectively. Each of the three excitations have both M_y (in-plane) and M_z (out-of-plane) fluctuations of the magnetic moments, which are differently modulated with \vec{Q} . In particular, we find that the characteristic “w” dispersion of the CEF envelope along the $(h, h, 0)$

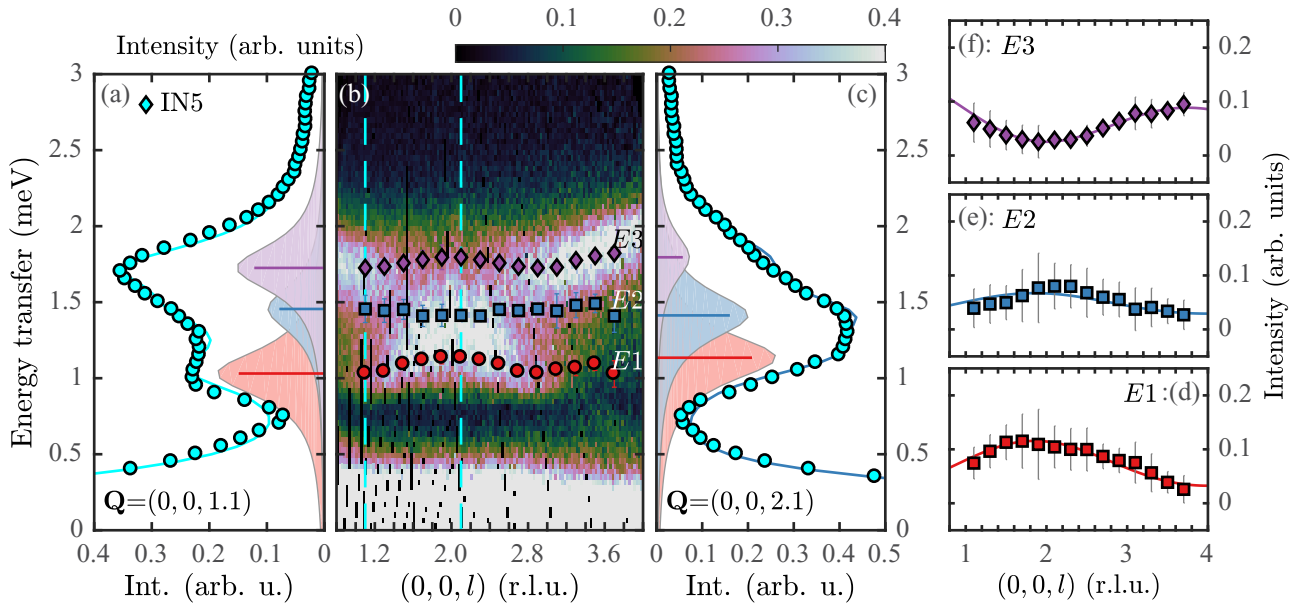


FIG. 7. The structure of the three exciton modes $E1$, $E2$, and $E3$ at $T = 0.07$ K, which develop from CEF1 at low temperature, along the $(0, 0, l)$ direction. (b) Shows a color map of the unpolarized time-of-flight neutron intensity. Cuts through the data along the cyan broken lines (TOF) are shown in (a) and (c). Three peaks were fitted to the unpolarized (TOF) data, as in Fig. 6 for the $(h, h, 0)$ direction, but here no polarized TAS data to directly evidence the three modes are available. The wave-vector dependence of the resulting intensities are shown in (d)–(f), where the lines are a guide to the eye. The extracted peak positions of the three exciton modes are the points superimposed on (b), and error bars on these positions are comparable to the symbol size.

direction in the unpolarized neutron spectrum is dominated by large intensities due to fluctuations of the magnetic moment M_z (i.e., fluctuations parallel to $[1\bar{1}0]$) in $E1$ and $E2$, shown in Figs. 9(g) and 9(h), and illustrated schematically in Fig. 9(e). The \vec{Q} dependence of the integrated intensities of the M_y fluctuations for modes $E2$ and $E3$ behave differently. The intensity of $E2$ is best described by a constant, while the intensity of $E3$ becomes anomalously large exactly at the Brillouin zone center $(2, 2, 0)$, the origin of the hybridization, as shown in Figs. 9(a)–9(c). However, we did not observe a clear indication of whether M_y or M_z fluctuations couple to the TAP to form the strongly dispersing MEM branches; rather, we found that all of the branches contain

wave-vector-dependent contributions from both types of transverse spin fluctuations.

E. Anisotropy of magnetoelastic fluctuations

When measuring the MEM at $(2, 2, 0)$, with $\vec{k} \parallel (h, h, 0)$, the spin components perpendicular to the scattering vector \vec{Q} are also transverse to \vec{k} , hence, we are studying a transverse mode. We find that the transverse fluctuations involve both in- and out-of-plane components, M_y and M_z , respectively, as can be seen in Fig. 2(b) where the signal appears in both P_y and P_z channels. However, it is also possible to measure the MEM at $(0, 0, 2)$, with $\vec{k} \parallel (h, h, 2)$. Now, as explained above

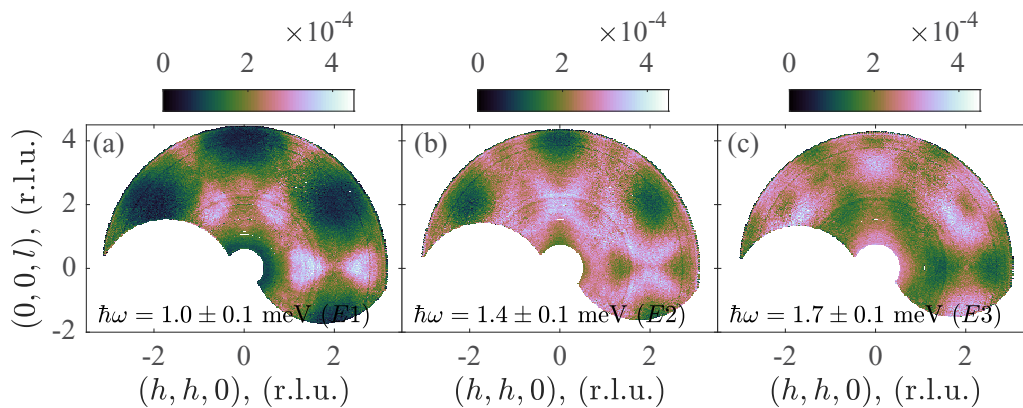


FIG. 8. Structure factor of the exciton branches. Considering the exciton branches to be dispersionless and therefore integrating them each within a narrow energy window [i.e., $\Delta(\hbar\omega) = \pm 0.1$ meV] in TOF data shows their wave-vector dependence. The cut in (a) is at 1.0 meV and is therefore dominated by the $E1$ exciton. (b), (c) Show cuts at 1.4 meV ($E2$) and 1.7 meV ($E3$), respectively.

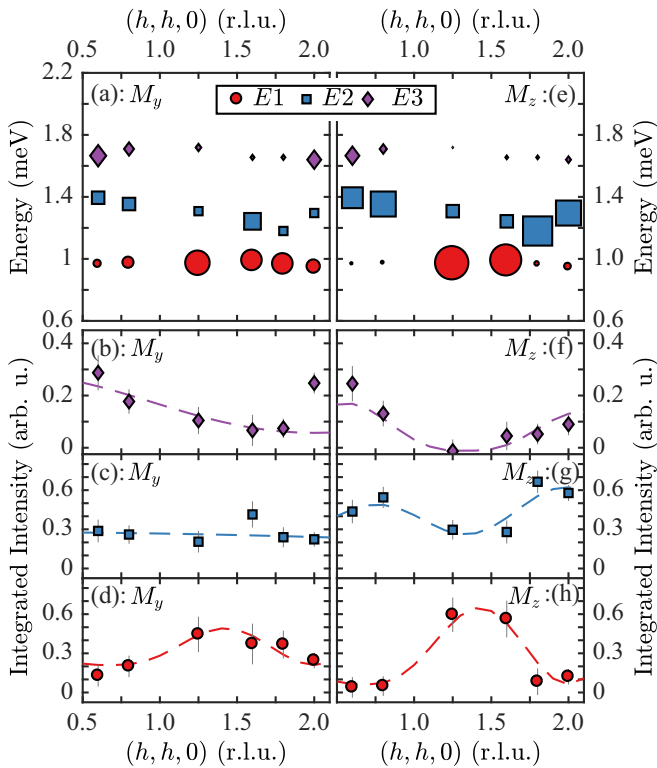


FIG. 9. Anisotropy and dispersion of magnetic fluctuations contributing to the MEM with $\vec{k} \parallel (h, h, 0)$ at $(2, 2, 0)$ (magnetic branch, M_y and M_z transverse), $(0, 0, 2)$ (magnetic branch, M_y longitudinal and M_z transverse) and $(0, 0, 8)$ (phonon branch). The orientation of \vec{Q} and \vec{k} , transverse and longitudinal magnetic fluctuations, and transverse phonon fluctuations are summarized in (a), as described in the Introduction and Fig. 1. In the other panels, shaded bars are for $\hbar\omega = 7$ meV and open bars are for $\hbar\omega = 5$ meV. At $(2, 2, 0)$ M_y is a transverse (T) fluctuation and contributes strongly (b), while at $(0, 0, 2)$ it is a longitudinal (L) fluctuation and makes essentially no contribution. M_z is a transverse fluctuation of approximately equal importance at both positions. Only nuclear/phonon scattering occurs at $(0, 0, 8)$ as can be seen by comparing intensities in P_x (nuclear) and P_x' (magnetic) channels (d).

and illustrated in Fig. 1, any in-plane fluctuations (M_y) that are perpendicular to the scattering vector \vec{Q} are parallel to the propagation direction \vec{k} and we therefore study the possibility of longitudinal spin fluctuations. The direct-space spin components contributing to these fluctuations are summarized in Table I.

In Fig. 10 we compare these possibilities using single-point intensity measurements at the peak of the different signals under investigation at $\hbar\omega = 5$ and 7 meV. At $(0, 0, 8)$, on the TAP, the magnetic and spin incoherent contributions are essentially zero, so all scattering appears in the P_x channel (and none in P_x'). At $(2, 2, 0)$ and $(0, 0, 2)$ we use the full polarization analysis to separate anisotropic magnetic, nuclear, and spin incoherent scattering. We see a significant M_y contribution at $(2, 2, 0)$, where it is a transverse fluctuation, but almost none at $(0, 0, 2)$ where it would be a longitudinal fluctuation. At $(2, 2, 0)$, the M_y contribution to the MEM is approximately twice the M_z contribution. The M_z contribution, which is always transverse, is the same at both positions.

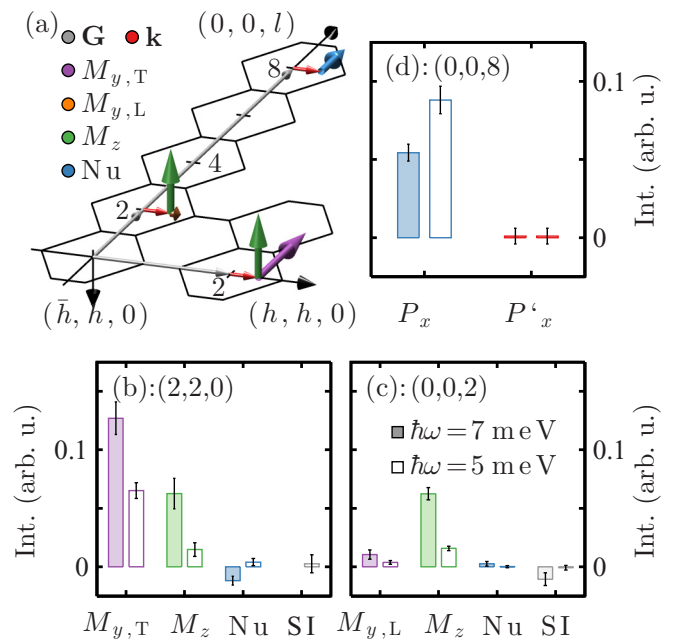


FIG. 10. Comparison of fluctuations contributing to the MEM with $\vec{k} \parallel (h, h, 0)$ at $(2, 2, 0)$ (magnetic branch, M_y and M_z transverse), $(0, 0, 2)$ (magnetic branch, M_y longitudinal and M_z transverse) and $(0, 0, 8)$ (phonon branch). The orientation of \vec{Q} and \vec{k} , transverse and longitudinal magnetic fluctuations, and transverse phonon fluctuations are summarized in (a), as described in the Introduction and Fig. 1. In the other panels, shaded bars are for $\hbar\omega = 7$ meV and open bars are for $\hbar\omega = 5$ meV. At $(2, 2, 0)$ M_y is a transverse (T) fluctuation and contributes strongly (b), while at $(0, 0, 2)$ it is a longitudinal (L) fluctuation and makes essentially no contribution. M_z is a transverse fluctuation of approximately equal importance at both positions. Only nuclear/phonon scattering occurs at $(0, 0, 8)$ as can be seen by comparing intensities in P_x (nuclear) and P_x' (magnetic) channels (d).

When we investigate the MEMs propagating along (h, h, h) at $(1, 1, 1)$ and $(0, 0, l)$ at $(0, 0, 2)$, such that M_y and M_z are both transverse fluctuations as at $(2, 2, 0)$, we find approximately equal contributions from both components at both positions, as shown in Fig. 11. Apparently, the magnetic fluctuations within the MEM are transverse to the propagation direction. They are anisotropic between $[001]$ and $[1\bar{1}0]$ [transverse M_y and M_z , respectively, when $\vec{k} \parallel (h, h, 0)$, Fig. 10(b)], but quite isotropic between $[\bar{1}\bar{1}2]$ and $[1\bar{1}0]$ (transverse M_y and M_z , respectively, when $\vec{k} \parallel (h, h, h)$, Fig. 11(a)). When measuring at $(0, 0, 2)$, the two polarization directions $[110]$ and $[1\bar{1}0]$ [transverse M_y and M_z , respectively, when $\vec{k} \parallel (0, 0, l)$, Fig. 11(b)] are equivalent and, consequently, the fluctuations have equal intensity.

V. DISCUSSION

Figure 12 summarizes our characterization of the magnetoelastic excitation spectrum of $\text{Tb}_2\text{Ti}_2\text{O}_7$ in zero magnetic field, particularly concerning modes with $\vec{k} \parallel (h, h, 0)$. In the figure we see the three exciton branches $E1, E2, E3$ of the CEF1 envelope, with their wave-vector-dependent intensity and anisotropy; the MEM and TAP with identical dispersions

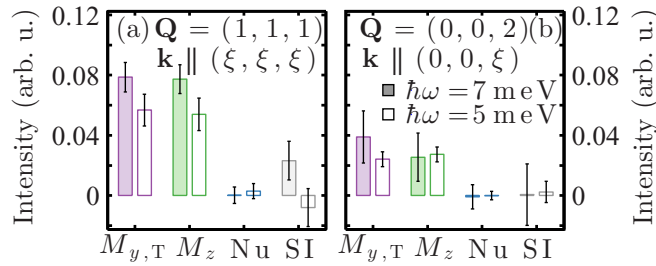


FIG. 11. Comparison of fluctuations contributing to the MEM with $\vec{k} \parallel (h, h, h)$ at $(1, 1, 1)$ (magnetic branch, M_y and M_z transverse) (a) and with $\vec{k} \parallel (0, 0, l)$ at $(0, 0, 2)$ (magnetic branch, M_y and M_z transverse) (b). Shaded bars are for $\hbar\omega = 7$ meV and open bars are for $\hbar\omega = 5$ meV. At both positions, the relationship between \vec{Q} and \vec{k} is analogous to that at $(2, 2, 0)$ in Fig. 1, so both M_y and M_z fluctuations are transverse (T) and contribute to the mode with approximately equal weight.

and different energy dependence of their intensities; and the anisotropy of the MEM [though we recall that this mode is rather more isotropic with $\vec{k} \parallel (0, 0, l)$ or $\vec{k} \parallel (h, h, h)$]. So far, we have presented experimental observations of these features, independent of any theory of $\text{Tb}_2\text{Ti}_2\text{O}_7$ but which should serve to constrain any such theory. However, we now discuss some interpretations: How does the excitation

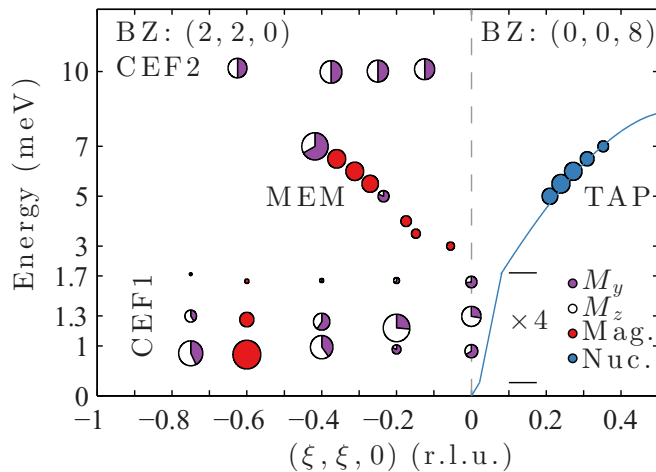


FIG. 12. Summary of the excitation spectrum in $\text{Tb}_2\text{Ti}_2\text{O}_7$ along the $(\xi, \xi, 0)$ direction of the reduced unit cell at $T = 0.07$ K. The magnetic part of the MEM appears in the Brillouin zone (BZ) of $(2, 2, 0)$ above the broad CEF1 envelope and follows the dispersion of the transverse-acoustic phonon (TAP), observed in the BZ $(0, 0, 8)$. The size of the marker symbols relates to the neutron intensity of each excitation, which are scaled among each other for the sake of representation. When available, the ratio of in-plane (M_y , shaded) and out-of-plane (M_z , open) polarization of the magnetic fluctuations is depicted by the partial shading of the symbol. Where polarization information is not available, a solid symbol is used to depict the intensity of magnetic or nuclear scattering. In order to emphasize the dispersion of the CEF1 doublet, the lower part of the y axis is enlarged by a factor of 4 between the black horizontal lines. The solid blue line represents the dispersion of the TAP propagating along the $(\xi, \xi, 0)$ direction, calculated using the finite displacement method [80].

spectrum of $\text{Tb}_2\text{Ti}_2\text{O}_7$ come to contain these features, and what, if anything, do they tell us about the low-temperature state of $\text{Tb}_2\text{Ti}_2\text{O}_7$ and its Hamiltonian? Our discussion has three particular themes that we have divided into subsections for clarity.

A. Overall structure of crystal field and magnetoelastic excitation spectrum in $\text{Tb}_2\text{Ti}_2\text{O}_7$

Previously [8], it was pointed out that with ground and first excited crystal field states dominated by $a_4|\pm 4\rangle \pm a_5|\mp 5\rangle$ and $b_5|\pm 5\rangle \mp b_4|\mp 4\rangle$ components, respectively, there are finite matrix elements between them for the operators J_{\pm}, J_x, J_y , and the quadrupole operators O_{xz} and O_{yz} . The finite matrix elements of $J_{x,y}$ and the quadrupole operators mean that excitations from the ground state to CEF1 are transverse spin fluctuations that can be mixed with transverse phonons. Strictly, this argument applies for $\vec{k} \parallel (h, h, h)$ where the fluctuations due to $J_{x,y}$ of a spin that is parallel to $[111]$ are accurately described as transverse. Generalization to take account of non-collinear local coordinate frames and lower-symmetry propagation directions is complicated, but seems unlikely to change the basic idea that dipolar and quadrupolar matrix elements mix spin and lattice fluctuations. Other features of the MEM that were found to be consistent with a coupling that is linear in the relevant operators are the frequency dependence of the intensity (particularly the vanishing intensity as $\hbar\omega \rightarrow 0$), and the temperature dependence of the intensity. Two excitons were distinguished and attributed to interactions.

The measurements described above allow various developments of this general picture. First, we have observed that there are three excitons, $E1, E2, E3$, and a MEM. Because of the four-sublattice crystal structure, there should be four excitons [42]. It is very appealing therefore to view the MEM as the fourth exciton, i.e., $E4$, which lies just above the others in energy but somehow picks up the dispersion of the TAP over a significant part of the Brillouin zone, while the other three remain quasidispersions. From a calculation based on a somewhat idealized crystal field scheme with Heisenberg exchange and dipolar interactions, and mixing of the two low-lying doublets attributed to the J_{\pm} matrix elements, Kao *et al.* formed a dispersion relation from the maximum intensity in the dynamical structure factor [42]. For $(h, h, 0)$ this creates a single dispersive feature that has a rather flat minimum around $(2, 2, 0)$ and jumps up (in energy) just below $(1, 1, 0)$ and above $(3, 3, 0)$, very similar to the feature we show in Fig. 6(b). Although they did not distinguish the individual excitons, they attributed the jump in energy to the shifting of maximum spectral weight between exciton branches, just as we found.

The region of the spectrum where the four modes meet could not be completely elucidated. The MEM, or putative $E4$ exciton, disperses steeply down into the CEF1 envelope [see Fig. 6(b) or 12], where the intensity of M_y fluctuations in $E3$ is anomalously large [Fig. 9(b)] and the MEM dispersion begins to deviate from the pure TAP dispersion (Fig. 12). Accurate measurements of the dispersion of the TAP are not possible here due to the large resolution volume of a thermal TAS and strong contribution from the excitons. However, on grounds of time-reversal symmetry, the coupling must vanish as $\hbar\omega \rightarrow 0$,

so that an uncoupled phonon and exciton should appear. This may explain our observations in this region: As the phonon drops below CEF1 with $\vec{k} \rightarrow 0$ and $\hbar\omega \rightarrow 0$, the coupling (and MEM) vanishes leaving the bare $E4$ exciton to turn above $E3$ at the zone center, where it is responsible for the enhanced magnetic (M_y) intensity observed there.

The intensity of the MEM grows as we follow its dispersion along $(h, h, 0)$ out of $(2, 2, 0)$, as far as $\vec{k} = (0.5, 0.5, 0)$ where $\hbar\omega_{\text{MEM}} \approx 7$ meV, as shown in Fig. 12. In this work, this was the furthest that we could follow it and still clearly distinguish it from CEF2 for the purpose of the intensity measurements presented in Fig. 5. Calculations show that this point is very close to the top of the dispersion of the TAP, which disperses weakly back down toward $\vec{k} = X$ at $(1, 1, 0)$ (Fig. 6 of Ref. [80]). However, according to Ref. [8], the MEM comes close to CEF2 (≈ 10 meV) but can be distinguished as a weak shoulder below it at $\hbar\omega \approx 8$ meV for $(0.5, 0.5, 0) < \vec{k} < (1, 1, 0)$ (Figs. 1 and 3 of Ref. [8]). Weak intensity from a transverse optical phonon that is just beneath CEF2 and approximately dispersionless across this region is predicted and has been observed [80], but it is unclear why $E4$ would first form a MEM with the TAP up to its dispersion maximum and then “transfer” its hybridization from the TAP to the optical phonon. There are some experimental signs that the width of the MEM is anomalous in this region, but these could not be precisely substantiated.

We note that along the $(h, h, 0)$ direction, there are two TAPs with different polarization vectors [i.e., TA1 with $\vec{e} = (0, 0, 1)$ and TA2 with $\vec{e} = (1, \bar{1}, 0)$], which are not degenerate. A different crystal orientation is required to access TA2 so we have not measured it in this work. However, since the identical dispersions of the magnetic and phononic parts are regarded as a key property of the hybridization, and TA2 has a different dispersion to TA1, it seems very likely that TA2 is not involved in the coupling because if it were, the magnetic part of the resulting hybrid mode should still be observable. If the crystal were reoriented to give [001] vertical, and an $(h, k, 0)$ scattering plane, we could observe TA2 at a position such as $\vec{Q} = (4, 4, 0)$, with $\vec{k} \parallel (h, \bar{h}, 0)$. In this case, the M_y (M_z) fluctuations of the associated MEM would be along the $[1\bar{1}0]$ ([001]) direction, just swapping the components between the polarization channels when compared to the experiments described above. The conditions for magnetic neutron scattering by a MEM involving TA2 would therefore be similarly favorable in either experiment, so the complete absence of a second MEM from all our data implies that TA2 does not hybridize with the crystal field excitons.

The agreement between the exciton band structure that we have observed and that calculated in Ref. [42] provides general support to the long-held hypothesis that the mixing of ground and first excited crystal field states by exchange and dipolar interactions is a crucial ingredient in the physics of $\text{Tb}_2\text{Ti}_2\text{O}_7$. However, a more detailed calculation of the individual excitons is required, and might allow determination of all the symmetry-allowed exchange interactions [50]. Quadrupolar terms would have to be incorporated to establish why the fourth exciton alone mixes with the TAP, what happens in the region where the TAP crosses the excitons, and

what happens in the region beyond the maximum of the TAP dispersion. Recent works employing quadrupole-quadrupole interactions via anisotropic superexchanges and restricting the available degrees of freedom to the ground-state doublet have investigated the low-temperature physics, where it may reasonably be claimed that the ground-state doublet is isolated [29,51–53]. However, our observation of an overall exciton dispersion closely similar to that discussed by Kao *et al.* [42] suggests that ignoring the admixture of excited states will ultimately be unrealistic. Furthermore, given the numerous couplings between phonons now catalogued in $\text{Tb}_2\text{Ti}_2\text{O}_7$ [CEF1 and TAP to produce the MEM discussed here, CEF1 and an overlying optical mode to give a magnetoelastic optical mode (MEOM [16]) observed by a terahertz spectroscopy experiment mentioned further below [83], CEF3 and an optical phonon to produce a MEOM as described in Ref. [16]], the importance of effective coupling of multipoles by phonons [84] should also be assessed.

B. Comparison with terahertz spectroscopy experiments

In recent terahertz spectroscopy measurements [83], four peaks were found in the THz spectrum: P0 ($\hbar\omega_{\text{P0}} = 1.37$ meV), P1 ($\hbar\omega_{\text{P1}} = 1.71$ meV), P2 ($\hbar\omega_{\text{P2}} = 2.08$ meV), and P3 ($\hbar\omega_{\text{P3}} = 2.78$ meV). The energies and temperature dependence of P0 and P2 suggests they are excitations between the members of the ground-state and CEF1 doublets, with equal splitting of each doublet due to magnetoelastic coupling. The temperature dependence of P1 is not definitive, and that of P3 is suggestive of the formation of a MEOM by coupling with a higher-energy phonon. At the zone center, we find $\hbar\omega_{E1} \approx 1$ meV, $\hbar\omega_{E2} \approx 1.4$ meV, and $\hbar\omega_{E3} \approx 1.7$ meV, so that $E2 = \text{P0}$ and $E3 = \text{P1}$. P2 was suggested to correspond to the MEM extrapolated to the zone center, but we do not resolve it there by neutron scattering, though it would correspond reasonably well with the bare $E4$ contribution to M_y proposed above. $E1$ is not observed in the terahertz spectroscopy experiment and P3 is not observed by neutron scattering. The absence of P3 may be because the low-lying optical phonon that is suggested to be involved in the MEOM has no neutron scattering cross section [80]. The two experiments do find four modes in total derived from CEF1 at the zone center, as we expect, though the absence of one mode (i.e., $E1$ and P2) from each experiment is surprising and the interpretations are different [i.e., at the zone center, two equally split doublets (P0–P3) and a MEOM in Ref. [83], or four excitons ($E1$ – $E4$) and unobservable MEOM in this work].

C. Comparison with related compounds

The three quasidispersionless exciton branches are somewhat surprising at first sight: their formation from the bare crystal field excitation is due to two-ion interactions, so why then do they not also become significantly dispersive, as in materials such as Pr [85,86] or HoF_3 [87]?

The structure factors of the three excitons shown in Fig. 8 each bear some resemblance to the structure factor of elastic scattering in various other model frustrated magnets. For $E1$ the pronounced triangles pointing in toward $(0, 0, 2)$ and,

particularly, (2, 2, 0) resemble the pyrochlore Heisenberg antiferromagnet [88–90]; for $E2$ the scattering is somewhat reminiscent of the pinch points and “butterflies” of intensity found in $\text{Tb}_2\text{Ti}_2\text{O}_7$ [37] or $\text{Tb}_2\text{Hf}_2\text{O}_7$ [91]; while for $E3$ the scattering around the boundary of the first zone, at (0, 0, 3) and around the boundary of the (2, 2, 2) zone is somewhat similar to a dipolar spin ice [92] or a tiling of hexagonal clusters on the pyrochlore lattice [93,94].

The appearance of localized modes with structure factors that can be phenomenologically identified with clusters on the pyrochlore lattice is not uncommon, even within magnetically ordered states, as in several spinels. The development of a flat band with nontrivial structure factor is a hallmark of localized magnon states, which are quite widely associated with quantum fluctuations and geometric frustration in diverse systems [95]. Although they develop from an existing crystal field excitation, excitons have much in common with magnons [96] in the sense of being propagating waves of angular momentum modification.

Perhaps of most relevance are rare-earth pyrochlores such as $\text{Nd}_2\text{Zr}_2\text{O}_7$ [97] or $\text{Pr}_2\text{Zr}_2\text{O}_7$ [98,99], although in both these cases the excitations in question are pure cooperative modes not derived from preexisting crystal field excitations. In the former, a dispersionless inelastic mode with spin ice structure factor was interpreted as a zero energy mode lifted to a finite energy by additional terms in the Hamiltonian. In the latter, calculation of the spin dynamics associated with the excitation revealed an ice rule in the phases of precession of the pseudospins and hence a nondivergent dynamical magnetization above the quadrupolar ground state. In $\text{Tb}_2\text{Ti}_2\text{O}_7$ it seems possible that the more complicated structure of the excitation spectrum in which the cooperative excitons are derived from interactions operating on a pair of crystal field doublets each with significant nonleading contributions (rather than interactions operating on thermally isolated, Ising-type doublets) could result in fluctuation modes with contrasting characters, i.e., the dynamics of different modes would be due to different

combinations of operators or (pseudo)spin components and hence resemble different spin models. It is interesting to speculate that the admixture of doublets that is evidenced by the general agreement with the calculation of Kao *et al.* [42] does indeed act to make $\text{Tb}_2\text{Ti}_2\text{O}_7$ a quantum spin ice mediated by virtual crystal field excitations, as proposed by Molavian *et al.* [43], and hence to inquire about the nature of localized exciton states in such a system.

VI. CONCLUSION

Using polarization analysis and measuring the MEMs in different directions, we could confirm that they are formed by the coupling of spin fluctuations derived from CEF1 with lattice fluctuations derived from the TAP. The spin fluctuations are dominantly transverse with respect to the direction of propagation. The hybridization that produces the magnetic branch develops at the energy scale of the thermal depopulation of CEF1, while the temperature and frequency dependence of the phonon branch show it is a rather classical phonon and only little perturbed by the hybridization. The CEF1 excitation develops into quasidispersionless excitons with distinctive and anisotropic structure factors, suggesting cooperative but localized excitations, mediated by interactions that are strong enough to span the gap from the ground state.

ACKNOWLEDGMENTS

We thank P. Santini for discussions, B. Vettard, X. Thonon, and M. Bartkowiak for assistance with cryogenics at IN22, IN14, and EIGER, respectively, and E. Villard for technical assistance at IN14. Neutron scattering experiments [100] were carried out at the Institut Laue Langevin in Grenoble, France; and SINQ at the Paul Scherrer Institut, Villigen PSI, Switzerland. Work at PSI was partly funded by the Swiss National Science Foundation (Grants No. 200021_140862 and No. 200020_162626).

-
- [1] J. S. Gardner, M. J. P. Gingras, and J. E. Greedan, *Rev. Mod. Phys.* **82**, 53 (2010).
 - [2] J. G. Rau and M. J. P. Gingras, *Annu. Rev. Condens. Matter Phys.* **10**, 022317 (2018).
 - [3] T. Taniguchi, H. Kadowaki, H. Takatsu, B. Fåk, J. Ollivier, T. Yamazaki, T. J. Sato, H. Yoshizawa, Y. Shimura, T. Sakakibara, T. Hong, K. Goto, L. R. Yaraskavitch, J. B. Kycia, *Phys. Rev. B* **87**, 060408(R) (2013).
 - [4] H. Kadowaki, M. Wakita, B. Fåk, J. Ollivier, S. Ohira-Kawamura, K. Nakajima, H. Takatsu, and M. Tamai, *J. Phys. Soc. Jpn.* **87**, 064704 (2018).
 - [5] H. Kadowaki, M. Wakita, B. Fåk, J. Ollivier, S. Ohira-Kawamura, K. Nakajima, and J. W. Lynn, *Phys. Rev. B* **99**, 014406 (2019).
 - [6] C. Castelnovo, R. Moessner, and S. L. Sondhi, *Annu. Rev. Condens. Matter Phys.* **3**, 35 (2012).
 - [7] M. J. P. Gingras and P. A. McClarty, *Rep. Prog. Phys.* **77**, 056501 (2014).
 - [8] T. Fennell, M. Kenzelmann, B. Roessli, H. Mutka, J. Ollivier, M. Ruminy, U. Stuhr, O. Zaharko, L. Bovo, A. Cervellino *et al.*, *Phys. Rev. Lett.* **112**, 017203 (2014).
 - [9] S. Guitteny, J. Robert, P. Bonville, J. Ollivier, C. Decorse, P. Steffens, M. Boehm, H. Mutka, I. Mirebeau, and S. Petit, *Phys. Rev. Lett.* **111**, 087201 (2013).
 - [10] M. J. P. Gingras, B. C. den Hertog, M. Faucher, J. S. Gardner, S. R. Dunsiger, L. J. Chang, B. D. Gaulin, N. P. Raju, and J. E. Greedan, *Phys. Rev. B* **62**, 6496 (2000).
 - [11] J. S. Gardner, B. D. Gaulin, A. J. Berlinsky, P. Waldron, S. R. Dunsiger, N. P. Raju, and J. E. Greedan, *Phys. Rev. B* **64**, 224416 (2001).
 - [12] I. Mirebeau, P. Bonville, and M. Hennion, *Phys. Rev. B* **76**, 184436 (2007).
 - [13] T. T. A. Lummen, I. P. Handayani, M. C. Donker, D. Fausti, G. Dhalenne, P. Berthet, A. Revcolevschi, and P. H. M. van Loosdrecht, *Phys. Rev. B* **77**, 214310 (2008).

- [14] J. Zhang, K. Fritsch, Z. Hao, B. V. Bagheri, M. J. P. Gingras, G. E. Granroth, P. Jiramongkolchai, R. J. Cava, and B. D. Gaulin, *Phys. Rev. B* **89**, 134410 (2014).
- [15] A. J. Princep, H. C. Walker, D. T. Adroja, D. Prabhakaran, and A. T. Boothroyd, *Phys. Rev. B* **91**, 224430 (2015).
- [16] M. Ruminy, E. Pomjakushina, K. Iida, K. Kamazawa, D. T. Adroja, U. Stuhr, and T. Fennell, *Phys. Rev. B* **94**, 024430 (2016).
- [17] S. T. Bramwell and M. J. Harris, *J. Phys.: Condens. Matter* **10**, L215 (1998).
- [18] R. Moessner, *Phys. Rev. B* **57**, R5587 (1998).
- [19] G. A. Gehring and K. A. Gehring, *Rep. Prog. Phys.* **38**, 1 (1975).
- [20] R. Siddharthan, B. S. Shastry, A. P. Ramirez, A. Hayashi, R. J. Cava, and S. Rosenkranz, *Phys. Rev. Lett.* **83**, 1854 (1999).
- [21] N. Hamaguchi, T. Matsushita, N. Wada, Y. Yasui, and M. Sato, *Phys. Rev. B* **69**, 132413 (2004).
- [22] A. Yaouanc, P. Dalmas de Réotier, Y. Chapuis, C. Marin, S. Vanishri, D. Aoki, B. Fåk, L.-P. Regnault, C. Buisson, A. Amato *et al.*, *Phys. Rev. B* **84**, 184403 (2011).
- [23] J. S. Gardner, S. R. Dunsiger, B. D. Gaulin, M. J. P. Gingras, J. E. Greedan, R. F. Kiefl, M. D. Lumsden, W. A. MacFarlane, N. P. Raju, J. E. Sonier *et al.*, *Phys. Rev. Lett.* **82**, 1012 (1999).
- [24] G. Luo, S. T. Hess, and L. R. Corruccini, *Phys. Lett. A* **291**, 306 (2001).
- [25] J. S. Gardner, A. Keren, G. Ehlers, C. Stock, E. Segal, J. M. Roper, B. Fåk, M. B. Stone, P. R. Hammar, D. H. Reich *et al.*, *Phys. Rev. B* **68**, 180401(R) (2003).
- [26] K. A. Ross, T. Proffen, H. A. Dabkowska, J. A. Quilliam, L. R. Yaraskavitch, J. B. Kycia, and B. D. Gaulin, *Phys. Rev. B* **86**, 174424 (2012).
- [27] H. Kadowaki, H. Takatsu, T. Taniguchi, B. Fåk, and J. Ollivier, *SPIN* **5**, 1540003 (2015).
- [28] M. Wakita, T. Taniguchi, H. Edamoto, H. Takatsu, and H. Kadowaki, *J. Phys.: Conf. Ser.* **683**, 012023 (2016).
- [29] H. Takatsu, S. Onoda, S. Kittaka, A. Kasahara, Y. Kono, T. Sakakibara, Y. Kato, B. Fåk, J. Ollivier, J. W. Lynn *et al.*, *Phys. Rev. Lett.* **116**, 217201 (2016).
- [30] H. Takatsu, T. Taniguchi, S. Kittaka, T. Sakakibara, and H. Kadowaki, *J. Phys.: Conf. Ser.* **683**, 012022 (2016).
- [31] H. Takatsu, T. Taniguchi, S. Kittaka, T. Sakakibara, and H. Kadowaki, *J. Phys.: Conf. Ser.* **828**, 012007 (2017).
- [32] H. Kadowaki, H. Takatsu, and M. Wakita, *Phys. Rev. B* **98**, 144410 (2018).
- [33] E. Kermarrec, D. D. Maharaj, J. Gaudet, K. Fritsch, D. Pomaranski, J. B. Kycia, Y. Qiu, J. R. D. Copley, M. M. P. Couchman, A. O. R. Morningstar *et al.*, *Phys. Rev. B* **92**, 245114 (2015).
- [34] H. Cao, A. Gukasov, I. Mirebeau, P. Bonville, and G. Dhaldenne, *Phys. Rev. Lett.* **101**, 196402 (2008).
- [35] H. Cao, A. Gukasov, I. Mirebeau, P. Bonville, C. Decorse, and G. Dhaldenne, *Phys. Rev. Lett.* **103**, 056402 (2009).
- [36] Y. Yasui, M. Kanada, M. Ito, H. Harashina, M. Sato, H. Okumura, K. Kakurai, and H. Kadowaki, *J. Phys. Soc. Jpn.* **71**, 599 (2002).
- [37] T. Fennell, M. Kenzelmann, B. Roessli, M. K. Haas, and R. J. Cava, *Phys. Rev. Lett.* **109**, 017201 (2012).
- [38] S. Petit, P. Bonville, J. Robert, C. Decorse, and I. Mirebeau, *Phys. Rev. B* **86**, 174403 (2012).
- [39] K. Fritsch, K. A. Ross, Y. Qiu, J. R. D. Copley, T. Guidi, R. I. Bewley, H. A. Dabkowska, and B. D. Gaulin, *Phys. Rev. B* **87**, 094410 (2013).
- [40] K. Fritsch, E. Kermarrec, K. A. Ross, Y. Qiu, J. R. D. Copley, D. Pomaranski, J. B. Kycia, H. A. Dabkowska, and B. D. Gaulin, *Phys. Rev. B* **90**, 014429 (2014).
- [41] S. Guitteny, I. Mirebeau, P. Dalmas de Réotier, C. V. Colin, P. Bonville, F. Porcher, B. Grenier, C. Decorse, and S. Petit, *Phys. Rev. B* **92**, 144412 (2015).
- [42] Y.-J. Kao, M. Enjalran, A. Del Maestro, H. R. Molavian, and M. J. P. Gingras, *Phys. Rev. B* **68**, 172407 (2003).
- [43] H. R. Molavian, M. J. P. Gingras, and B. Canals, *Phys. Rev. Lett.* **98**, 157204 (2007).
- [44] H. R. Molavian and M. J. P. Gingras, *J. Phys.: Condens. Matter* **21**, 172201 (2009).
- [45] P. J. Baker, M. J. Matthews, S. R. Giblin, P. Schiffer, C. Baines, and D. Prabhakaran, *Phys. Rev. B* **86**, 094424 (2012).
- [46] S. Legl, C. Krey, S. R. Dunsiger, H. A. Dabkowska, J. A. Rodriguez, G. M. Luke, and C. Pfleiderer, *Phys. Rev. Lett.* **109**, 047201 (2012).
- [47] E. Lhotel, C. Paulsen, P. D. de Réotier, A. Yaouanc, C. Marin, and S. Vanishri, *Phys. Rev. B* **86**, 020410(R) (2012).
- [48] L. Yin, J. S. Xia, Y. Takano, N. S. Sullivan, Q. J. Li, and X. F. Sun, *Phys. Rev. Lett.* **110**, 137201 (2013).
- [49] A. P. Sazonov, A. Gukasov, H. B. Cao, P. Bonville, E. Ressouche, C. Decorse, and I. Mirebeau, *Phys. Rev. B* **88**, 184428 (2013).
- [50] S. H. Curnoe, *Phys. Rev. B* **88**, 014429 (2013).
- [51] S. Onoda and Y. Tanaka, *Phys. Rev. Lett.* **105**, 047201 (2010).
- [52] S. Onoda and Y. Tanaka, *Phys. Rev. B* **83**, 094411 (2011).
- [53] S. B. Lee, S. Onoda, and L. Balents, *Phys. Rev. B* **86**, 104412 (2012).
- [54] M. Hermele, M. P. A. Fisher, and L. Balents, *Phys. Rev. B* **69**, 064404 (2004).
- [55] O. Benton, O. Sikora, and N. Shannon, *Phys. Rev. B* **86**, 075154 (2012).
- [56] K. A. Ross, L. Savary, B. D. Gaulin, and L. Balents, *Phys. Rev. X* **1**, 021002 (2011).
- [57] P. Bonville, I. Mirebeau, A. Gukasov, S. Petit, and J. Robert, *Phys. Rev. B* **84**, 184409 (2011).
- [58] P. Bonville, A. Gukasov, I. Mirebeau, and S. Petit, *Phys. Rev. B* **89**, 085115 (2014).
- [59] S. W. Han, J. S. Gardner, and C. H. Booth, *Phys. Rev. B* **69**, 024416 (2004).
- [60] J. P. C. Ruff, B. D. Gaulin, J. P. Castellan, K. C. Rule, J. P. Clancy, J. Rodriguez, and H. A. Dabkowska, *Phys. Rev. Lett.* **99**, 237202 (2007).
- [61] K. Goto, H. Takatsu, T. Taniguchi, and H. Kadowaki, *J. Phys. Soc. Jpn.* **81**, 015001 (2012).
- [62] P. Dalmas de Réotier, A. Yaouanc, A. Bertin, C. Marin, S. Vanishri, D. Sheptyakov, A. Cervellino, B. Roessli, and C. Baines, *J. Phys.: Conf. Ser.* **551**, 012021 (2014).
- [63] M. Ruminy, F. Groitl, T. Keller, and T. Fennell, *Phys. Rev. B* **94**, 174406 (2016).
- [64] K. C. Rule and P. Bonville, *J. Phys.: Conf. Ser.* **145**, 012027 (2009).
- [65] B. D. Gaulin, J. S. Gardner, P. A. McClarty, and M. J. P. Gingras, *Phys. Rev. B* **84**, 140402(R) (2011).

- [66] L. G. Mamsurova, K. S. Pigalskii, and K. K. Pukhov, Pis'ma Zh. Eksp. Teor. Fiz. **43**, 584 (1986) [JETP Lett. **43**, 755 (1986)].
- [67] L. G. Mamsurova, K. S. Pigalskii, and K. K. Pukhov, Zh. Eksp. Teor. Fiz. **94**, 209 (1988) [Sov. Phys.–JETP **67**, 550 (1988)].
- [68] Y. Nakanishi, T. Kumagai, M. Yoshizawa, K. Matsuhira, S. Takagi, and Z. Hiroi, *Phys. Rev. B* **83**, 184434 (2011).
- [69] S. Kitani, M. Tachibana, and H. Kawaji, *Solid State Commun.* **247**, 94 (2016).
- [70] I. Mirebeau, I. N. Goncharenko, P. Cadavez-Pares, S. T. Bramwell, M. J. P. Gingras, and J. S. Gardner, *Nature (London)* **420**, 54 (2002).
- [71] I. Mirebeau, I. N. Goncharenko, G. Dhalenne, and A. Revcolevschi, *Phys. Rev. Lett.* **93**, 187204 (2004).
- [72] J. P. C. Ruff, Z. Islam, J. P. Clancy, K. A. Ross, H. Nojiri, Y. H. Matsuda, H. A. Dabkowska, A. D. Dabkowski, and B. D. Gaulin, *Phys. Rev. Lett.* **105**, 077203 (2010).
- [73] K. C. Rule, J. P. C. Ruff, B. D. Gaulin, S. R. Dunsiger, J. S. Gardner, J. P. Clancy, M. J. Lewis, H. A. Dabkowska, I. Mirebeau, P. Manuel, Y. Qiu, and J. R. D. Copley, *Phys. Rev. Lett.* **96**, 177201 (2006).
- [74] M. Ruminy, L. Bovo, E. Pomjakushina, M. K. Haas, U. Stuhr, A. Cervellino, R. J. Cava, M. Kenzelmann, and T. Fennell, *Phys. Rev. B* **93**, 144407 (2016).
- [75] H. Takatsu, H. Kadowaki, T. J. Sato, J. W. Lynn, Y. Tabata, T. Yamazaki, and K. Matsuhira, *J. Phys.: Condens. Matter* **24**, 052201 (2011).
- [76] See Supplemental Material at <http://link.aps.org/supplemental/10.1103/PhysRevB.99.224431> for the comparison of the inelastic neutron scattering spectra, and heat capacities, of our samples.
- [77] F. Tasset, P. J. Brown, E. Lelièvre-Berna, T. Roberts, S. Pujol, J. Allibon, and E. Bourgeat-Lami, *Phys. B (Amsterdam)* **267**, 69 (1999).
- [78] L. P. Regnault, B. Geffray, P. Fouilloux, B. Longuet, F. Mantegezza, F. Tasset, E. Lelièvre-Berna, E. Bourgeat-Lami, M. Thomas, and Y. Gibert, *Phys. B (Amsterdam)* **335**, 255 (2003).
- [79] U. Stuhr, B. Roessli, S. Gvasaliya, H. M. Ronnow, U. Filges, D. Graf, A. Bollhalder, D. Hohl, R. Burge, M. Schild *et al.*, *Nucl. Instrum. Methods Phys. Res., Sect. A* **853**, 16 (2017).
- [80] M. Ruminy, M. N. Valdez, B. Wehinger, A. Bosak, D. T. Adroja, U. Stuhr, K. Iida, K. Kamazawa, E. Pomjakushina, D. Prabhakaran *et al.*, *Phys. Rev. B* **93**, 214308 (2016).
- [81] M. Popovici, *Acta Crystallogr. Sect. A* **31**, 507 (1975).
- [82] D. A. Tennant and D. F. McMorrow, RESCAL for MATLAB: A computational package for calculating neutron TAS resolution functions (1995).
- [83] E. Constable, R. Ballou, J. Robert, C. Decorse, J. B. Brubach, P. Roy, E. Lhotel, L. Del-Rey, V. Simonet, S. Petit *et al.*, *Phys. Rev. B* **95**, 020415(R) (2017).
- [84] P. Santini, S. Carretta, G. Amoretti, R. Caciuffo, N. Magnani, and G. H. Lander, *Rev. Mod. Phys.* **81**, 807 (2009).
- [85] J. G. Houman, M. Chapellier, A. R. Mackintosh, P. Bak, O. D. McMasters, and K. A. Gschneidner, Jr., *Phys. Rev. Lett.* **34**, 587 (1975).
- [86] J. G. Houmann, B. D. Rainford, J. Jensen, and A. R. Mackintosh, *Phys. Rev. B* **20**, 1105 (1979).
- [87] M. J. M. Leask, M. R. Wells, R. C. C. Ward, S. M. Hayden, and J. Jensen, *J. Phys.: Condens. Matter* **6**, 505 (1994).
- [88] B. Canals and D. Garanin, *Can. J. Phys.* **79**, 1323 (2001).
- [89] S. V. Isakov, K. Gregor, R. Moessner, and S. L. Sondhi, *Phys. Rev. Lett.* **93**, 167204 (2004).
- [90] C. L. Henley, *Phys. Rev. B* **71**, 014424 (2005).
- [91] R. Sibille, E. Lhotel, M. C. Hatnean, G. J. Nilsen, G. Ehlers, A. Cervellino, E. Ressouche, M. Frontzek, O. Zaharko, V. Pomjakushin *et al.*, *Nat. Commun.* **8**, 892 (2017).
- [92] S. R. Giblin, M. Twengström, L. Bovo, M. Ruminy, M. Bartkowiak, P. Manuel, J. C. Andresen, D. Prabhakaran, G. Balakrishnan, E. Pomjakushina *et al.*, *Phys. Rev. Lett.* **121**, 067202 (2018).
- [93] S.-H. Lee, C. Broholm, W. Ratcliff, G. Gasparovic, Q. Huang, T. H. Kim, and S.-W. Cheong, *Nature (London)* **418**, 856 (2002).
- [94] T. Yavors'kii, T. Fennell, M. J. P. Gingras, and S. T. Bramwell, *Phys. Rev. Lett.* **101**, 037204 (2008).
- [95] O. Derzhko, J. Richter, and M. Maksymenko, *Int. J. Mod. Phys. B* **29**, 1530007 (2015).
- [96] B. Grover, *Phys. Rev.* **140**, A1944 (1965).
- [97] S. Petit, E. Lhotel, B. Canals, M. Ciomaga Hatnean, J. Ollivier, H. Mutka, E. Ressouche, A. R. Wildes, M. R. Lees, and G. Balakrishnan, *Nat. Phys.* **12**, 746 (2016).
- [98] S. Petit, E. Lhotel, S. Guitteny, O. Florea, J. Robert, P. Bonville, I. Mirebeau, J. Ollivier, H. Mutka, E. Ressouche *et al.*, *Phys. Rev. B* **94**, 165153 (2016).
- [99] N. Martin, P. Bonville, E. Lhotel, S. Guitteny, A. Wildes, C. Decorse, M. Ciomaga Hatnean, G. Balakrishnan, I. Mirebeau, and S. Petit, *Phys. Rev. X* **7**, 041028 (2017).
- [100] T. Fennell, S. Guitteny, S. Petit, M. Boehm, M. Kenzelmann, I. Mirebeau, J. Robert, B. Roessli, M. Ruminy, and P. Steffens, (2013), doi: 10.5291/ILL-DATA.4-01-1240.